



**HAL**  
open science

# How the Binder/Solvent Formulation Impacts the Electrolyte Reactivity/Solid Electrolyte Interphase Formation and Cycling Stability of Conversion Type Electrodes

Lénaïc Madec, Gaël Coquil, Jean-Bernard Ledeuil, Grégory Gachot, Laure Monconduit, Hervé Martinez

► **To cite this version:**

Lénaïc Madec, Gaël Coquil, Jean-Bernard Ledeuil, Grégory Gachot, Laure Monconduit, et al.. How the Binder/Solvent Formulation Impacts the Electrolyte Reactivity/Solid Electrolyte Interphase Formation and Cycling Stability of Conversion Type Electrodes. *Journal of The Electrochemical Society*, 2020, 167 (6), pp.060533. 10.1149/1945-7111/ab861f. hal-02567268

**HAL Id: hal-02567268**

**<https://hal.umontpellier.fr/hal-02567268>**

Submitted on 12 Nov 2020

**HAL** is a multi-disciplinary open access archive for the deposit and dissemination of scientific research documents, whether they are published or not. The documents may come from teaching and research institutions in France or abroad, or from public or private research centers.

L'archive ouverte pluridisciplinaire **HAL**, est destinée au dépôt et à la diffusion de documents scientifiques de niveau recherche, publiés ou non, émanant des établissements d'enseignement et de recherche français ou étrangers, des laboratoires publics ou privés.

**How the binder/solvent formulation impacts the electrolyte reactivity/solid electrolyte interphase formation and cycling stability of conversion type electrodes**

Lénaïc Madec,<sup>1,4,\*</sup> Gaël Coquil,<sup>2</sup> Jean-Bernard Ledeuil,<sup>1</sup> Grégory Gachot,<sup>3,4</sup> Laure Monconduit,<sup>2,4</sup> and Hervé Martinez<sup>1,4</sup>

<sup>1</sup> CNRS/ UNIV Pau & Pays Adour/ E2S UPPA, Institut des Sciences Analytiques et de Physicochimie pour l'Environnement et les Matériaux, UMR5254, 64000, Pau, France

<sup>2</sup> ICG-AIME, Bat 15, cc 15-02, Université Montpellier 2, Pl. E. Bataillon, 34095 Montpellier cedex 5, France

<sup>3</sup> Laboratoire de Réactivité et Chimie des Solides (LRCS), CNRS, UMR 7314, Université de Picardie Jules Verne, 33 rue Saint Leu, Amiens, France

<sup>4</sup> Réseau sur le Stockage Electrochimique de l'Energie (RS2E), CNRS FR3459, 33 Rue Saint Leu, 80039 Amiens Cedex, France

\* Corresponding Author: E-mail: lenaic.madec@univ-pau.fr

**ABSTRACT**

Conversion/alloying type materials are of great interests in term of electrochemical performance for Li-ion batteries and beyond. To address their large volume change (typically >200%) during cycling, tailoring the binder/solvent system used for the electrode formulation together with the use of electrolyte additives are the most used and efficient approaches. However, only few studies have investigated the role of the binder/solvent formulation on the electrolyte reactivity/solid electrolyte interphase (SEI) formation and its composition. To tackle this issue, gas chromatography coupled with electron impact mass spectrometry and X-ray photoelectron spectroscopy analysis were used to understand the long term cycling stability (100 cycles) of NbSnSb-based electrodes. It is showed that CMC-H<sub>2</sub>O and PAA-H<sub>2</sub>O

formulations favored the formation of a more homogeneous SEI while maintaining efficient active/conducting particles bridging, which results in high cycling stability. PVDF-NMP and PAA-NMP led, however, to much lower coulombic efficiency and higher irreversible capacity correlated with the formation of thick SEI with a concomitant disconnection of active particles. These results highlight that CMC and PAA act as artificial SEI and/or as SEI stabilizers. Overall, this work should benefit to all researchers working on improving, through electrode formulation, the lifetime of Li-ion batteries and beyond.

## **INTRODUCTION**

Conversion/alloying type materials have revolutionized Li-ion and beyond in term of electrochemical performance and fundamental aspect. However, they suffer from large volume change (typically >200%) during cycling, which can lead to particles pulverization, loss of electrical contact<sup>1</sup> and continuous electrolyte consumption due to the solid electrolyte interphase (SEI) breaking/reforming.<sup>2</sup> For conversion materials, composite made of electrochemically active/inactive elements vs. lithium have been successfully developed to buffer the volume change.<sup>2,3</sup> However, to address these drawbacks at once, tailoring the binder/solvent system used for the conversion/alloy-based electrode formulation is probably the most efficient approach.<sup>4,5</sup> Ideally, the binder should allow bridging the active and conductive particles surface and forming strong interactions with the active particles surface while keeping its mechanical properties. This was successfully performed in the case of Si electrodes formulated with sodium carboxymethyl cellulose (CMC) in acidic water solution.<sup>6,7</sup> The use of highly elastic binder with self-healing properties is also an efficient approach.<sup>8</sup> For conversion materials, CMC also greatly enhanced the performance compared to polyvinylidene fluoride (PVDF)<sup>9</sup> or polyacrylic acid sodium salt (PAA).<sup>10</sup> These results were explained by the formation of a more efficient active/conducting particles bridging via the CMC rather than from a better volume change buffering during cycling. The improved cycle life was also attributed

to the formation of a more efficient SEI thanks to the better active particles covering by the CMC. In other words, the binder acts as an ‘artificial’ SEI at the active particles surface or as a SEI stabilizer,<sup>11</sup> similarly to electrolyte additives, but as soon as the electrode is formulated. Using this approach, Li<sup>+</sup> was reversibly intercalated into graphite in propylene carbonate.<sup>12,13,14</sup> However, only few studies have investigated the binder impact on SEI formation and its composition. In the case of both Li<sub>4</sub>Ti<sub>5</sub>O<sub>12</sub><sup>15</sup> and graphite,<sup>16</sup> thicker SEI were observed with PAA compared to CMC when formulated in water. Moreover, PAA and CMC-based graphite electrodes led to the formation of more carboxylates and alkoxides than PVDF, due to the water formulation while PAA also led to more electrolyte salt degradation.<sup>16</sup>

Based on these considerations, this study aims at understand the impact of the binder/solvent formulation on the electrolyte reactivity / SEI formation and resulting electrochemical performance of NbSnSb-based electrodes cycled at 25°C in 1M LiPF<sub>6</sub> EC:PC:3DMC + 5% FEC + 1% VC. In that way, gas chromatography coupled with electron impact mass spectrometry (GC/MS) and X-ray photoelectron spectroscopy (XPS) are used to correlate the electrolyte reactivity and SEI passivation/stability/composition with the stability over 100 cycles.

## **EXPERIMENTAL**

NbSnSb was prepared following a previously described procedure.<sup>17</sup> Note that the same batch of NbSnSb powder was used to prepare the different electrodes presented in this study. Four electrodes formulations were prepared by varying the binder/solvent system, namely sodium carboxymethyl cellulose (CMC, DS = 0.7, Mw ~250 000, Aldrich) or polyacrylic acid sodium salt (PAA, Mw ~2 100, Sigma Aldrich) with deionized water (H<sub>2</sub>O) and PAA (Mw ~2 100, Sigma Aldrich) or polyvinylidene fluoride (PVDF, Mw ~1 000 000, Solef) with *N*-Methyl-2-

pyrrolidone (NMP, anhydrous, 99,5%, Sigma Aldrich), referred to as CMC-H<sub>2</sub>O, PAA-H<sub>2</sub>O, PAA-NMP and PVDF-NMP, respectively. Electrodes were prepared by mixing 70:9:9:12 weight ratio of NbSnSb:acetylene black (Super P, BET = 62 m<sup>2</sup>/g, TIMCAL):vapor ground carbon fibers (VGCF-S, BET = 15 m<sup>2</sup>/g, Showa Denko)V:binder in the corresponding solvent using a silicon nitride vial and a planetary ball-milling for 1 h. The weight of the dry mass was 430 mg in 0.8 ml of H<sub>2</sub>O or 1 ml of NMP and the number of balls was 4 with a 5 mm diameter. Slurries were tape casted on a 17.5 μm thick copper foil (99.9 %, Goodfellow) with a 150 μm thickness. After drying for 48 h at room temperature then 15 h at 120°C under vacuum, electrodes of 12.7 mm diameter were punched out. Note that for CMC-H<sub>2</sub>O and PAA-H<sub>2</sub>O, the active mass loading was 2.5 mg<sub>NbSnSb</sub>/cm<sup>2</sup> ±0.2 mg while it was 1.25 mg<sub>NbSnSb</sub>/cm<sup>2</sup> ±0.2 mg for PAA-NMP and PVDF-NMP. Electrode porosity was about 65% for all binder/solvent systems. 2032 NbSnSb/Li coin cells were assembled using as electrolyte, 0.225 ml of 1 M LiPF<sub>6</sub> in EC:PC:3DMC (99.9%, Solvionic) with a 1:1:3 vol ratio + 5 % FEC (≥ 98.5% purity, Aldrich) + 1 % VC (≥ 99%, Alfa Aesar) in volume. A glass-fiber paper (GF/D, Whatman) and a polypropylene-polyethylene-polypropylene (PPP) membrane separator (Celgard) were used as separators at the Li and NbSnSb electrodes side, respectively. Cycling was performed using a Neware Battery Testing System between 0.02-1.5 V vs. Li<sup>+</sup>/Li at 25°C with a first C/2 discharge (i.e. 0.5 mole of Li per mole of NbSnSb per hour) followed by a 48 h storage at 0.02 V then 100 cycles at 4C (i.e. 320 mA/g), stopped in charge. After cells opening, separators and NbSnSb electrodes were used for GC/MS and XPS analysis, respectively. Corresponding analysis conditions can be found in details in previous studies.<sup>18</sup> For clarity, NbSnSb electrodes were washed twice by immersion in DMC (anhydrous, ≥99% purity, Aldrich, 1 ml) in a clean and dry glass vial with a mild manual agitation (10s).

## RESULTS AND DISCUSSION

## Cycling stability vs. electrolyte reactivity

Figure 1 shows the long term cycling stability of NbSnSb/Li coin cells as function of the binder/solvent system. For clarity, for each system, data for only one cell is presented. Overall, the capacity retention (Figure 1a) followed: CMC-H<sub>2</sub>O > PAA-H<sub>2</sub>O >> PVDF-NMP ≈ PAA-NMP. This result appears surprising as the active mass loading was two times higher for CMC-H<sub>2</sub>O and PAA-H<sub>2</sub>O (2.5 mg<sub>NbSnSb</sub>/cm<sup>2</sup> ± 0.3 mg) compared to PAA-NMP and PVDF-NMP (1.25 mg<sub>NbSnSb</sub>/cm<sup>2</sup> ± 0.2 mg). Indeed, the increase of the active mass loading usually leads to lower capacity retention, especially in the case of conversion material.<sup>10</sup> In the present case, the large and rapid capacity drop of PAA-NMP and PVDF-NMP, especially over the first 10 cycles, can be explained by their much lower initial coulombic efficiency (CE, Figure 1b) and concomitant higher relative irreversible capacity (relative IRC) (Figure 1c). This latter was calculated as: relative IRC = IRC/D<sub>n</sub> = (D<sub>n</sub>-D<sub>n+1</sub>)/D<sub>n</sub> where D<sub>n</sub> and D<sub>n+1</sub> are the discharge capacities at cycle n and n+1, respectively. These results suggest that NMP-based formulations lead to the rapid formation of SEI and the concomitant disconnection of active particles. This is in good agreement with the relative IRC associated with the disconnection of active particles (IRC<sub>disconnection</sub> = (C<sub>n</sub>-C<sub>n+1</sub>)/C<sub>n</sub> where C<sub>n</sub> and C<sub>n+1</sub> are the charge capacities at cycle n and n+1, respectively<sup>19</sup>) that showed a rapid and large increase, especially over the first 10 cycles, compared to H<sub>2</sub>O-based formulations.

The mole of consumed electrons was then calculated from the IRC as mol<sub>IRC</sub> = m<sub>elec</sub> \* IRC<sub>100cycles</sub> \* 3.6/F where m<sub>elec</sub> is the electrode weight in mg, IRC<sub>100cycle</sub> the cumulative IRC after 100 cycles and F the Faraday constant (96485 C/mol). Considering that the mole of consumed electrons after 100 cycles (Table 1) should be associated with the electrolyte additives consumption (*i.e.* the FEC and VC reduction), thus the additives consumption should thus follow: CMC-H<sub>2</sub>O > PAA-H<sub>2</sub>O > PVDF-NMP > PAA-NMP. This hypothesis was confirmed by GC/MS analysis of the electrolytes after cycling (Figure 2). Indeed, the

chromatograms of the electrolytes extracted after 100 cycles from NbSnSb/Li coin cells as function of the binder/solvent system showed a consumption of the FEC and VC additives compared to fresh electrolyte and the observed consumptions followed the calculated mole of consumed electrons ( $\text{mol}_{\text{IRC}}$ ). Notes that reproducibility was checked with duplicate cells but are not presented for clarity. However, Table 1 shows that for all binder/solvent systems, the mole of consumed additives (from the GC/MS, knowing the electrolyte volume and composition in the cells) was about 2.2 times higher than the mole of consumed electrons. Thus, the mole of consumed electrons appears greatly underestimated due to: (i) the use of lithium metal that may consumed electrolyte additives; (ii) the additives consumption during the charge, due to SEI cracking/repair due to the particles deflation, which is not accounted for<sup>19</sup> and (iii) the partial additives consumption through chemical reactions. However, this latter phenomenon, being in principle associated to the lithium alkoxides (ROLi) trapping, would involve the DMC reduction into ROLi<sup>20</sup> and thus consumed an equivalent number of electron. Also, the preferential VC/FEC reduction is well known to prevent the reduction of linear carbonates and the associated generation of lithium alkoxides.<sup>20</sup> Moreover, considering the surface area of a Li metal electrode, the additives consumption associated with its passivation is likely negligible, especially considering that no visible dendrite formation was observed after 100 cycles (not shown). In any case, the electrolyte and Li metal being the same for all cells, any difference in additives consumption has to come from the additives reactivity at the NbSnSb electrode. Overall, the much higher number of moles of consumed additives compared to the number of moles of consumed electrons is therefore explained by the additives consumption during charge as the SEI is damaged by the particles deflation then repaired as the fresh surface is exposed to the electrolyte. Interestingly, this conclusion is supported by the evolution of the mole of reversible capacity after 100 cycles (Table 1). This latter was calculated as follows:

$$\text{mol}_{\text{RC}} = (D_{100\text{cycles}} - \text{IRC}_{100\text{cycles}}) * m_{\text{elec}} * 3.6/F$$
 where  $D_{100\text{cycles}}$  is the cumulative discharge capacity

after 100 cycles. Indeed,  $\text{mole}_{\text{RC}}$  followed the amount of consumed additives so that the larger active particles inflation/deflation leads to a larger additives consumption.

### **SEI passivation/stability and composition**

The SEI passivation/stability and its composition was then investigated using XPS analysis of the electrodes surface. Figure 3 shows the XPS core spectra for elements of interest (C and O) while Table 2 shows the full XPS quantification including the peaks attribution based on our previous study.<sup>18</sup>

After cycling, the Nb, Sn and Sb peaks from the active material, the C=C peak from the carbon additives as well as the peaks (*i.e.* Na and C-F) from the binders significantly decreased. These phenomena were, however, much more pronounced in the case of NMP-based formulations indicating the formation of thicker SEI at their electrodes surface despite the lower additives consumption. These results therefore suggest an accumulation of SEI species at the electrodes surface for NMP-based formulations, in agreement with their lower CE and higher IRC, especially over the first 10 cycles (Figure 1b and c). This can also explain the rapid and large active particles disconnection (Figure 1d). It also suggests a more homogeneous distribution of SEI species over the whole electrode thickness in the case of H<sub>2</sub>O-based formulations due to the low active particles disconnection (Figure 1d) that leads to a continuous SEI cracking/repair during the particles swelling/deflation. Overall, these results highlight the role of the binder/solvent system: *i.e.* CMC-H<sub>2</sub>O and PAA-H<sub>2</sub>O formulations favor a homogeneous SEI formation while maintaining efficient active/conducting particles bridging over the entire cycling. Therefore, CMC and PAA binders appear to act as artificial SEI and/or as SEI stabilizer. CMC-H<sub>2</sub>O leads, however, to improved cycling stability compared to PAA-H<sub>2</sub>O, which could be related to the much higher Mw of the CMC, in agreement with the literature.<sup>10</sup> Note that for PAA-NMP, much lower amount of -CO<sub>2</sub> and associated Na (from the PAA) were observed at the pristine electrode surface compared to PAA-H<sub>2</sub>O (Table 2), indicating a partial

binder degradation during the electrode formulation. This result explains the lower cycling stability of PAA-NMP as the much lower amount of  $-\text{CO}_2\text{Na}$  groups may lead to poor bond with the active particles surface and thus to poor active/conducting particles bridging. The poor cycling stability with PVDF-NMP is also believed to originate from poor bond with the active particles surface and concomitant poor active/conducting particles bridging.

Considering the SEI composition, the formation of an oligomer of VC was observed for all binder/solvent systems except for PAA-NMP (Figure 3 and Table 2), likely due to the very low VC consumption for this formulation (Figure 2). Interestingly, the amount of LiF (Table 2) follows the consumption of the FEC (Figure 2):  $\text{CMC-H}_2\text{O} \gg \text{PAA-H}_2\text{O} > \text{PVDF-NMP} > \text{PAA-NMP}$ . This result suggests that LiF is preferentially formed from the reduction of  $\text{FEC}^{20,21,22}$  rather than from the  $\text{LiPF}_6$  degradation in aqueous formulation. This latter thus appears greatly hindered by the use of electrolyte additives and their passivation of the SEI, in agreement with the relatively low amount of  $\text{PO}_x$ ,  $\text{PO}_x\text{F}_y$  and  $\text{PF}_x$  observed ( $<1$  at.% in total, Table 2).

## CONCLUSIONS

In this study, the role of the binder/solvent formulation on the electrolyte reactivity/SEI formation and resulting cycling stability was highlighted in the case of NbSnSb-based conversion type electrode (cycled with 1M  $\text{LiPF}_6$  EC:PC:3DMC + 5% FEC + 1% VC) using GC/MS and XPS analysis. Overall, the capacity retention followed:  $\text{CMC-H}_2\text{O} > \text{PAA-H}_2\text{O} \gg \text{PVDF-NMP} \approx \text{PAA-NMP}$ . This was explained by the much lower CE and higher IRC for NMP-based formulations that led to a rapid formation of thick SEI with a concomitant disconnection of active particles. For  $\text{H}_2\text{O}$ -based formulations, however, the binders favored the formation of a more homogeneous SEI while maintaining efficient active/conducting particles bridging.

CMC and PAA thus act as artificial SEI and/or as SEI stabilizer. Moreover, the poor cycling stability with PAA-NMP and PVDF-NMP more likely originated from a poor bonding with the active particles surface and thus from poor active/conducting particles bridging.

Interestingly, the electrolyte additives consumption followed the amount of moles of consumed electrons. This latter was, however, underestimated due to the SEI cracking/repair that consumed additives during the particles deflation over charge. Moreover, an oligomer of VC was observed by XPS except for PAA-NMP due to its very low VC consumption. Interestingly, the formation of LiF originated from the FEC consumption and the use of additives greatly limited the LiPF<sub>6</sub> degradation.

Overall, this work should benefit to all researchers working on improving, through electrode formulation, the lifetime of Li-ion batteries and beyond.

## **Acknowledgment**

This research was performed in the framework of “Réseau sur le Stockage Electrochimique de l’Energie” (RS2E) and the ANR program no. ANR-10-LABX-76-01. Authors thank Total S.A. and ADEME for the financial support of G. Coquil’s PhD Thesis and the fruitful discussions.

## **REFERENCES**

1. L. Y. Beaulieu, K. W. Eberman, R. L. Turner, L. J. Krause, and J. R. Dahn, *Electrochem. Solid-State Lett.*, **4**, A137–A140 (2001).
2. V. Aravindan, Y. S. Lee, and S. Madhavi, *Adv. Energy Mater.*, **5**, 1402225 (2015).
3. A. Mukhopadhyay and B. W. Sheldon, *Prog. Mater. Sci.*, **63**, 58–116 (2014).

4. B. Lestriez, *Comptes Rendus Chim.*, **13**, 1341–1350 (2010).
5. D. Guy, B. Lestriez, R. Bouchet, and D. Guyomard, *J. Electrochem. Soc.*, **153**, A679–A688 (2006).
6. N. S. Hochgatterer, M. R. Schweiger, S. Koller, P. R. Raimann, T. Wöhrle, C. Wurm, and M. Winter, *Electrochem. Solid-State Lett.*, **11**, A76 (2008).
7. D. Mazouzi, B. Lestriez, L. Roué, and D. Guyomard, *Electrochem. Solid-State Lett.*, **12**, A215–A218 (2009).
8. S. Choi, T. woo Kwon, A. Coskun, and J. W. Choi, *Science (80-. )*, **357**, 279–283 (2017).
9. V. Sivasankaran, C. Marino, M. Chamas, P. Soudan, D. Guyomard, J. C. Jumas, P. E. Lippens, L. Monconduit, and B. Lestriez, *J. Mater. Chem.*, **21**, 5076 (2011).
10. H. A. Wilhelm, C. Marino, A. Darwiche, P. Soudan, M. Morcrette, L. Monconduit, and B. Lestriez, *J. Power Sources*, **274**, 496–505 (2015).
11. Z. Karkar, D. Guyomard, L. Roué, and B. Lestriez, *Electrochim. Acta*, **258**, 453–466 (2017).
12. S. Komaba, K. Okushi, T. Ozeki, H. Yui, Y. Katayama, T. Miura, T. Saito, and H. Groult, *Electrochem. Solid-State Lett.*, **12**, A107 (2009).
13. S. Komaba, T. Ozeki, and K. Okushi, *J. Power Sources*, **189**, 197–203 (2009).
14. S. Komaba, N. Yabuuchi, T. Ozeki, K. Okushi, H. Yui, K. Konno, Y. Katayama, and T. Miura, *J. Power Sources*, **195**, 6069–6074 (2010).
15. T. Nordh, F. Jeschull, R. Younesi, T. Koçak, C. Tengstedt, K. Edström, and D. Brandell, *ChemElectroChem*, **4**, 2683–2692 (2017).
16. F. Jeschull, J. Maibach, R. Félix, M. Wohlfahrt-Mehrens, K. Edström, M. Memm, and D.

Brandell, *ACS Appl. Energy Mater.* (2018).

17. G. Coquil, M. T. Sougrati, S. Biscaglia, D. Aymé-Perrot, P. F. Girard, and L. Monconduit, *Electrochim. Acta*, **281**, 619–623 (2018).

18. L. Madec, G. Gachot, G. Coquil, H. Martinez, and L. Monconduit, *J. Power Sources*, **391**, 51–58 (2018).

19. M. Gauthier, D. Mazouzi, D. Reyter, B. Lestriez, P. Moreau, D. Guyomard, L. Roué, and L. Roue, *Energy Environ. Sci.*, **6**, 2145–2155 (2013).

20. R. Petibon, V. L. Chevrier, C. P. Aiken, D. S. Hall, S. R. Hyatt, R. Shunmugasundaram, and J. R. Dahn, *J. Electrochem. Soc.*, **163**, A1146–A1156 (2016).

21. K. Leung, S. B. Rempe, M. E. Foster, Y. Ma, J. M. M. Del La Hoz, N. Sai, and P. B. Balbuenab, *J. Electrochem. Soc.*, **161**, 3–11 (2014).

22. C. Xu, F. Lindgren, B. Philippe, M. Gorgoi, F. Björefors, K. Edström, and T. Gustafsson, *Chem. Mater.*, **27**, 2591–2599 (2015).

Figure 1.

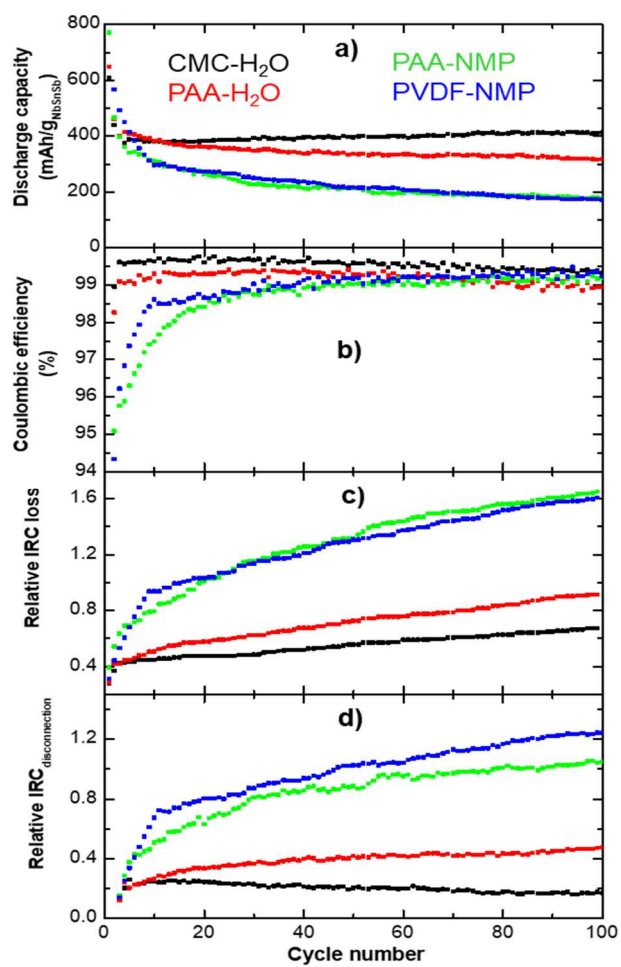


**Figure 2.**

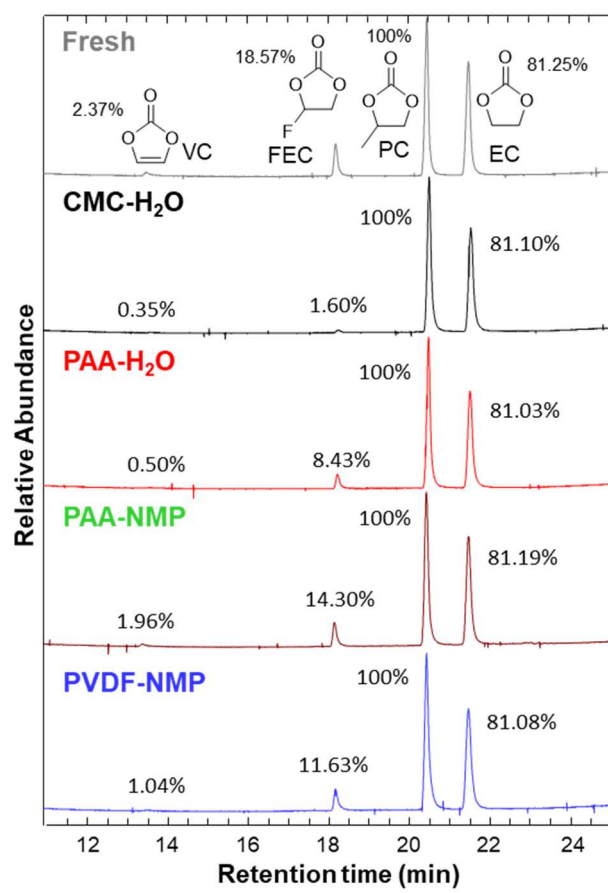
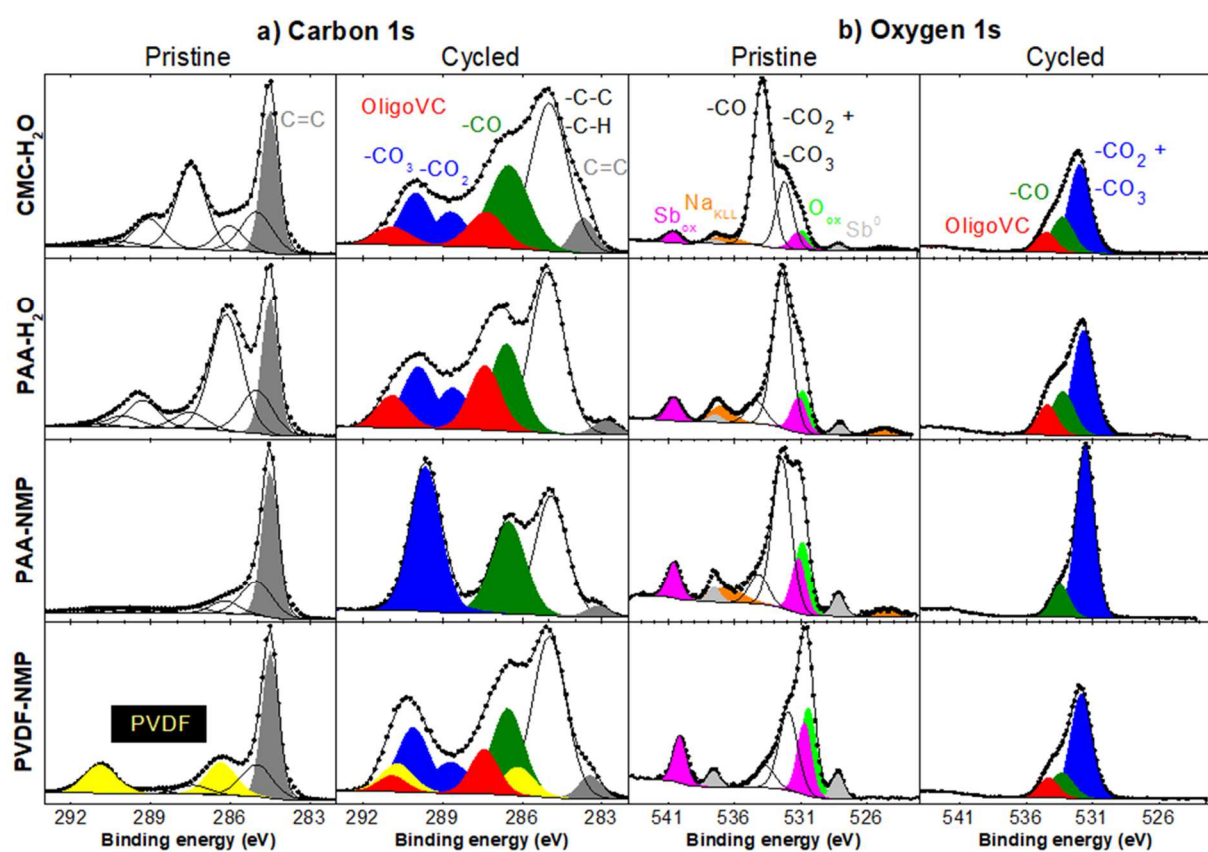


Figure 3.



**Table 1.**

|   | CMC<br>H <sub>2</sub> O | PAA<br>H <sub>2</sub> O | PAA<br>NMP | PVDF<br>NMP |
|---|-------------------------|-------------------------|------------|-------------|
| mole of consumed electrons (mole <sub>IRC</sub> )<br>*10 <sup>5</sup>   | 5.7                     | 3.9                     | 1.7        | 3.2         |
| mole of consumed additives (mole <sub>GC/MS</sub> )<br>*10 <sup>5</sup> | 13.7                    | 9.0                     | 3.4        | 6.2         |
| ratio<br>mole <sub>GC/MS</sub> /mole <sub>IRC</sub>                     | 2.4                     | 2.3                     | 2          | 1.9         |
| mole of reversible capacity (mole <sub>RC</sub> ) *10 <sup>4</sup>      | 5 <sup>1</sup>          | 3 <sup>2</sup>          | 5.9        | 11          |

**Table 2.**

|              |   |                    | CMC-H <sub>2</sub> O<br>Pristine | PAA-H <sub>2</sub> O<br>Pristine | PAA-NMP<br>Pristine | PVDF-NMP<br>Pristine | CMC-H <sub>2</sub> O<br>100 cycles | PAA-H <sub>2</sub> O<br>100 cycles | PAA-NMP<br>100 cycles | PVDF-NMP<br>100 cycles |
|--------------|---|--------------------|----------------------------------|----------------------------------|---------------------|----------------------|------------------------------------|------------------------------------|-----------------------|------------------------|
|              |   | B.E. (eV)          | At. %                            | At. %                            | At. %               | At. %                | At. %                              | At. %                              | At. %                 | At. %                  |
| <b>Nb 3d</b> | Nb metal  | 203.4-206.2        | 0.06                             | 0.12                             | 0.03                | 0.02                 | 0.01                               | -                                  | -                     | -                      |
|              | Nb oxide  | 206.2-209.0        | 0.5                              | 1.1                              | 0.3                 | 0.2                  | 0.01                               | -                                  | -                     | -                      |
| <b>Sn 3d</b> | Sn metal  | 484.2-492.6        | 0.07                             | 0.14                             | 0.05                | 0.01                 | 0.01                               | 0.05                               | -                     | -                      |
|              | Sn oxide  | 486.0-494.4        | 0.8                              | 1.9                              | 0.5                 | 0.3                  | 0.01                               | -                                  | -                     | -                      |
| <b>Sb 3d</b> | Sb metal  | 528.1-537.6        | 0.07                             | 0.14                             | 0.05                | 0.03                 | -                                  | -                                  | -                     | -                      |
|              | Sb oxide  | 531.2-540.6        | 0.3                              | 0.5                              | 0.14                | 0.12                 | -                                  | -                                  | -                     | -                      |
| <b>C 1s</b>  | <b>C=C</b>  | <284.5             | 19.9                             | 15.2                             | 49.6                | 30.2                 | 1.7                                | 0.9                                | -                     | 1.3                    |
|              | -CC, -CH  | 285.0              | 10.7                             | 9.7                              | 22.9                | 13.2                 | 12.2                               | 13.5                               | 9.8                   | 13.3                   |
|              | -CO   | 286.6              | 5.7                              | 25.8                             | 7.5                 | -                    | 7.3                                | 7.0                                | 7.9                   | 6.7                    |
|              | -CH (PVDF)  | 286.3              | -                                | -                                | -                   | 12.4                 | -                                  | -                                  | -                     | 2.2                    |
|              | -CO (CMC/PAA)                                       | 287.4              | 20.9                             | 3.7                              | 3.7                 | 3.7                  | -                                  | -                                  | -                     | -                      |
|              | -CO <sub>2</sub>                                    | 288.9              | 6.9                              | 6.1                              | 2.3                 | 1.6                  | 2.6                                | 3.4                                | 0.9                   | 2.9                    |
|              | -CO <sub>3</sub> (Li <sub>2</sub> CO <sub>3</sub> ) | 289.9              | 1.5                              | 2.7                              | 2.4                 | -                    | 3.6                                | 4.9                                | 11.7                  | 5.1                    |
|              | -CF (PVDF)  | 290.8              | -                                | -                                | -                   | 12.4                 | -                                  | -                                  | -                     | 2.2                    |
|              | π-π*  | 291.2              | 1.1                              | 0.8                              | 3.1                 | -                    | -                                  | -                                  | -                     | -                      |
|              | <b>OligoVC</b>                                      | <b>287.5-291.5</b> | -                                | -                                | -                   | -                    | <b>4.2</b>                         | <b>7.6</b>                         | -                     | <b>4.2</b>             |
| <b>O 1s</b>  | Nb, Sn, Sb oxides                                   | 530.9              | 1.8                              | 3.7                              | 1.3                 | 1.0                  | -                                  | -                                  | -                     | -                      |
|              | -CO <sub>3</sub> , CO <sub>2</sub>                  | 531.7              | 6.6                              | 15.3                             | 3.2 (+0.5eV)        | 1.1                  | 16.1                               | 19.3                               | 32.3                  | 19.5                   |
|              | -CO   | 533.4              | 17.7                             | 2.3                              | 0.6 (+0.7 eV)       | 0.3                  | 6.6                                | 8.4                                | 5.9                   | 5.0                    |
|              | <b>OligoVC</b>                                      | <b>534.3</b>       | -                                | -                                | -                   | -                    | <b>3.3</b>                         | <b>5</b>                           | -                     | <b>3.5</b>             |
| <b>F 1s</b>  | <b>LiF</b>  | 684.9              | -                                | -                                | -                   | -                    | 10.8                               | 3.6                                | 0.9                   | 2.6                    |
|              | LiPF <sub>6</sub> , PVDF                            | >686.9             | -                                | -                                | -                   | 23.4                 | 0.8                                | 1.6                                | 3.0                   | 5.1                    |

|              |                                |             |     |      |      |      |      |      |      |      |
|--------------|--------------------------------|-------------|-----|------|------|------|------|------|------|------|
| <b>Cl 2p</b> |                                | 198.4-200.0 | 0.1 | 0.1  | 0.03 | 0.02 | 0.18 | 0.08 | 0.1  | 0.13 |
| <b>Li 1s</b> | Total                          | 55.3        | -   | -    | -    | -    | 29.8 | 24.2 | 26.2 | 25.9 |
| <b>P 2p</b>  | PO <sub>x</sub>                | 133.4-134.3 | -   | -    | -    | -    | 0.19 | 0.17 | 0.3  | 0.2  |
|              | PO <sub>x</sub> F <sub>y</sub> | 134.7-135.6 | -   | -    | -    | -    | -    | 0.03 | -    | 0.04 |
|              | PF <sub>x</sub>                | 136.8-137.7 | -   | -    | -    | -    | 0.09 | 0.2  | 0.4  | 0.13 |
| <b>Na 1s</b> | Na (CMC/PAA)                   | -           | 5.3 | 10.7 | 2.3  | -    | 0.5  | 0.07 | 0.6  | -    |

**Figure 1.** a) Discharge capacity (mAh/gNbSnSb), b) coulombic efficiency, c) relative irreversible capacity (IRC) and d) relative IRC associated with the disconnection of active particles (IRCdisconnection) versus cycling number for NbSnSb/Li coin cells cycled at 25°C between 0.02-1.5 V at 4C using 1M LiPF<sub>6</sub> EC:PC:3DMC + 5% FEC + 1% VC as function of the binder/solvent system. Notes that reproducibility was checked with duplicate cells but are not presented for clarity.

**Figure 2.** Chromatograms of the fresh electrolyte and electrolytes extracted from NbSnSb/Li coin cells after 100 cycles at 25°C between 0.02-1.5 V at 4C using 1M LiPF<sub>6</sub> EC:PC:3DMC + 5% FEC + 1% VC as function of the binder/solvent system. The relative abundance of each solvent/additive, in %, was normalized relatively to PC. Notes that reproducibility was checked with duplicate cells but are not presented for clarity.

**Figure 3.** a) Carbon 1s and b) Oxygen 1s XPS core spectra of pristine and cycled NbSnSb electrodes after 100 cycles at 25°C using 1M LiPF<sub>6</sub> EC:PC:3DMC + 5% FEC + 1% VC as function of the binder/solvent system. Core level spectra of pristine electrodes were maximized to show low intensity peaks while for cycled electrodes, core level spectra were normalized to show the relative amount of a given element between samples.

**Table 1.** Number of moles of consumed electrons ( $\text{mole}_{\text{IRC}}$  from the IRC) and consumed additives ( $\text{mole}_{\text{GC/MS}}$  from the GC/MS), ratio between the number of  $\text{mole}_{\text{GC/MS}}$  and that of  $\text{mole}_{\text{IRC}}$  as well as mole of reversible capacity ( $\text{mole}_{\text{RC}}$ ) for NbSnSb/Li coin cells after 100 cycles as function of the binder/solvent system.

**Table 2.** XPS quantification data (in at.%) of pristine and cycled NbSnSb electrodes after 100 cycles at 25°C using 1M LiPF<sub>6</sub> EC:PC:3DMC + 5% FEC + 1% VC as function of the binder/solvent system.